Vol.23, No.4, PP.1-16 P-ISSN: 2070-4003 E-ISSN: 2664-5548

Computational Approach to the Study of Photon Radiation Shielding Parameters of Perovskite Ceramics

Muhammed Abdurraheem^{1*}, Sunday Ajani¹, Wasiu Yahya^{1,2}, and Godwin Egbeyale¹

¹Department of Physics and Materials Science, Kwara State University, Malete, Kwara, Nigeria

²Department of Physics, University of Ilorin, Ilorin, Nigeria

*Corresponding author: abdurraheemlayimuhammed@gmail.com

Abstract

This work investigates the photon radiation shielding efficiency of selected perovskite ceramics, halide-based double perovskites and organic-inorganic halide perovskites, using computational modeling across the photon energy range 0.015-15 MeV. The investigated parameters are Mass Attenuation Coefficient (MAC), Linear Attenuation Coefficient (LAC), Half Value Layer (HVL), Tenth Value Layer (TVL) and Mean Free Path (MFP). The results are based on the total interaction cross section contributions of photon-matter interactions. They reveal that the shielding efficiency of these materials is strongly influenced by their elemental composition, density, and photon energy. Two software tools, Phy-X/PSD and NGCal, were employed in the study to verify the accuracy of the calculations. The results from the two software tools are found to be in good agreement, with a difference in values of less than 0.1%. Halidebased double perovskites exhibited superior attenuation properties at low and intermediate photon energies due to their high-Z elements and relatively high density, while organic-inorganic halide perovskites displayed moderate shielding efficiency, limited mainly by lower density and lighter elemental composition. Yet, they remained attractive due to their tunability and potential for lightweight shielding applications. Overall, halide double perovskites offered the most promising radiation shielding performance among the studied materials. In particular, those containing heavy atoms, such as Pt (Z = 78), stand out as excellent photon-shielding candidates. Therefore, perovskite ceramics have significant potential as next-generation photon shielding materials. Future research should focus on experimental synthesis and long-term stability under radiation exposure to accelerate the practical deployment of perovskite ceramics in radiation applications.

Article Info.

Keywords:

Radiation Shielding,
Perovskite Ceramics,
Photon Attenuation,
Linear Attenuation
Coefficient,
Computational Approach

Article history:

Received: Oct. 03, 2025 Revised: Nov. 09, 2025 Accepted: Nov. 15, 2025 Published: Dec. 01, 2025

1. Introduction

Radiation induces deterioration to life, environment and electronic gadgets [1]. Photon-emitting radionuclides in diagnostic imaging techniques, and the exposure of patients, medical staff and the environment to potentially harmful ionizing radiation in the form of X-rays and gamma rays during nuclear power generation have extensively exposed individuals to potentially harmful ionizing radiation [2-6]. However, conventional radiation shielding materials, such as lead and concrete, have been widely used as reliable and efficient shielding materials but suffer from significant drawbacks, such as toxicity, environmental and human hazards, extreme weight and bulk, and variations in moisture content in concrete [1-3, 7]. As many technologies start to rely on radiation for operation, materials with high attenuation efficiency, mechanical stability, and environmental compatibility are required to ensure safety of life and environment, and operational effectiveness [1]. Moreover, conventional radiation shielding materials such as lead and concrete have been widely used as reliable and efficient shielding materials, but suffer from significant drawbacks such as toxicity, environmental and human hazard, extremely heavy and bulky, and moisture variation content in concrete [3,

7-9]. This required an urgent attention to design and development of an alternative shielding material with high attenuation efficiency combined with mechanical stability, chemical durability, light weight, non-toxicity, environmental safety, and friendliness [10, 11].

In past years, many compositions have been proposed and studied for radiation shielding purposes, such as glass, alloy, polymers [7, 8], and perovskite ceramics [11, 12]. Glass is transparent, non-toxic, easily shaped, but brittle and has low density; alloys have high density, strong mechanical properties but are heavy and often contain toxic elements. While polymer is lead-free, it has reduced environmental and health risks, but prolonged radiation exposure can cause polymer chains to break down, leading to discoloration, brittleness, or reduced mechanical strength [3, 7, 13]. Perovskite ceramics have gained significant attention as potential materials for radiation shielding due to their unique crystal structure, high density, structural flexibility, high atomic number, thermal and chemical stability, non-toxicity, and light weight. Halide-based double perovskites are a subclass of perovskite materials where the standard ABX₃ perovskite structure is modified into an A₂BB'X₆. They are inorganic halide perovskites that offer unique constituents of high-Z elements, structural tunability, high density, good mechanical and thermal stability, making it an exceptional material for photon radiation shielding [3, 7, 13, 14]. Moreover, organic-inorganic halide perovskites are semiconductor materials that combine organic and inorganic components in a perovskite-like crystal structure. They have a general formula of ABX₃, and have outstanding advantages due to their structural, chemical and optoelectrical properties, such as 1.5 eV direct wide optical band gap, 1000 nm diffusion length, long minority carrier life time, high absorption coefficient (10⁵ cm⁻¹), high dielectric constant, low cost, and flexible; they are highly used in technological applications [15]. In this study, photon radiation shielding capability of two classes of perovskite ceramics, halide-based double and organic-inorganic halide, was investigated in order to have an excellent and most promising material that can be used in nuclear medicine and engineering applications. Halide double perovskites are rarely explored for radiation shielding, despite their high density and heavy elements constituents.

2. Materials and Methods

Two classes of perovskite materials, halide-based double perovskite (Cs₂SnI₆, Cs₂TiI₆, Cs₂TiI₆, Cs₂HfI₆, Cs₂TeI₆, Cs₂PtI₆, Cs₂PtI₆, Cs₂PdI₆) and organic-inorganic halide perovskite (CH₃NH₃PbI₃, CH₃NH₃PbBr₃ CH₃NH₃SnI₃, HC(NH₂)₂SnI₃, HC(NH₂)₂PbI₃) were selected for radiation shielding purposes. Their photon radiation shielding parameters, Mass Attenuation Coefficient (MAC), Linear Attenuation Coefficient (LAC), Half Value Layer (HVL), Tenth Value Layer (TVL) and Mean Free Path (MFP) were studied across the energy range 0.015 - 15 MeV using Phy-X/PSD (version 9.17.524) and NGCal (version 100.18.000.1026) software. The survey energy range was chosen because it encompasses the three most dominant photon-matter interaction mechanisms: photoelectric effect (0 - 0.1 MeV), Compton scattering (0.1 -3 MeV) and pair production (3 -15 MeV), which determine the material's radiation shielding parameters. This makes the study comprehensive and comparable to international standards, allowing for the accurate modeling and design of effective perovskite-based shielding solutions [24].

The most crucial factor describing how radiation passes through various materials is the attenuation coefficient, which enables the derivation of all radiation shielding parameters [17, 19]. The incident intensity of radiation decreases when a parallel beam of photons traverses a material, resulting in different radiation interaction mechanisms, such as photoelectric effect, Compton scattering, and pair production [17, 15]. These events depend directly on the atomic number of the target material and the energy of the

incident photons. However, photons travel at a considerable distance before transferring their partial or all energy to the target material electron [15].

The Beer-Lambert law describes the relationship between the transmitted and incident photon intensity as expressed in Eq. (1) [18]:

$$I\left(x\right) = I_0 e^{-\mu x} \tag{1}$$

where I(x) is the transmitted intensity or attenuated photon intensity or intensity of the radiation after passing through a material of thickness x, I_0 is the initial or incident intensity or unattenuated photon intensity, μ is the linear attenuation coefficient of the material (cm⁻¹) and x is the thickness of the material (cm).

2. 1. Linear attenuation coefficient (LAC)

LAC is the characteristic of a material that describes how much a beam of photons (X-ray or gamma ray) is attenuated per unit thickness of a material [16]. It depends on the atomic composition of the material, its density, and the energy of the incident photons [12, 21]. LAC is obtained from Lambert-Beer's law as expressed in Eq. (2) [12]:

$$\mu = -\ln\left(\frac{l}{l_0}\right)\frac{1}{x} \tag{2}$$

2. 2. Mass Attenuation Coefficient (MAC)

MAC is a measure of how effectively a material can attenuate (absorb or scatter) photon radiation per unit mass. Its variation is not directly dependent on density, but strongly depends on photon energy and the atomic number of the material. It is expressed in Eq. (3) as [2]:

$$\mu_m = -\frac{1}{\rho x} \ln \left(\frac{I}{I_0} \right) \tag{3}$$

The relationship between LAC and MAC is given as Eq. (4) [17]:

$$\mu = \mu_m \times \rho \tag{4}$$

where ρ is the density of material and μ_m is the mass attenuation coefficient.

In case of a multi-element material, such as chemical compound or homogeneous mixture establishing the sample, the MAC can be acquired from the weighted sum of the coefficients for the elements as expressed in Eq. (5) [19]:

$$\left(\frac{\mu}{\rho}\right)_{i \ compound} = \sum_{i} w_{i} \left(\frac{\mu}{\rho}\right)_{i} \tag{5}$$

where $\left(\frac{\mu}{\rho}\right)_i$ is the MAC for the *i*-th constituent, w_i is the weight fraction for the *i*-th element, as given in Eq. (6) [20]:

$$w_i = \frac{n_i A_i}{M} \tag{6}$$

Where n_i is the number of atoms of i-th element in the compound, A_i is the atomic mass of the compound in g/mol and $M = \sum n_i A_i$ and is the molar mass of the compound in g/mol.

MAC is the most important parameter, as it is the quantity that most clearly indicates the shielding characteristics of an absorber material and suggests the possibility of photon-matter interactions [12, 15].

2. 3. Half Value Layer (HVL)

It is the thickness of material required to reduce photon radiation intensity by 50% or to half of its original value [5, 16]. It is expressed as the composite depth of the shielding material that transmits half of the incident photon beam intensity [2, 10, 19, 21]. It provides information about the thickness of a material that are suitable for radiation shielding. A low value of HVL indicates that a thin material is required to reduce the photon intensity by 50% [22]. The lower the HVL value of the composite, the better its shielding ability against hazardous radiation [6]. HVL is obtained from Beer-Lambert law as expressed in Eq. (7) [22]:

$$HVL = \frac{\ln 2}{\mu} \tag{7}$$

$$HVL = \frac{0.693}{\mu}$$

2. 4. Tenth Value Layer (TVL)

It is the thickness of a shielding material required to attenuate photon radiation intensity to one tenth of its original value or by 90% [2, 16, 19, 21]. Following Lambert-Beer's law, TVL can be expressed as Eq. (9) [22]:

$$TVL = \frac{\ln 10}{\mu}$$
 (9)

$$TVL = \frac{2.303}{\mu} \tag{10}$$

Therefore, HVL and TVL are related by Eq. (11):

$$TVL \approx 3.32 \times HVL \tag{11}$$

This indicates that TVL is approximately 3.32 times the HVL. Thus, each TVL provides significantly more attenuation.

2. 5. Mean Free Path (MFP)

It is the average distance a photon travels before colliding with the atoms of the target material via absorption, scattering or other processes [21, 5]. It depends on the nature of the material and the energy of the photon. Lower MFP values indicate that the material has superior attenuation properties [16, 19]. It is obtained following Lambert-Beer's law as expressed in Eq. (12) [22]:

$$\lambda = \frac{1}{\mu} \tag{12}$$

or
$$\lambda = \frac{1}{\mu} = \frac{1}{\left(\frac{\mu}{\rho}\right)\rho} \tag{13}$$

For a large attenuation coefficient material, photons interact more frequently, leading to a shorter MFP. Conversely, for a small LAC material, photons travel longer distances before interaction [16, 17].

2. 6. Atomic Cross-section (ACS)

ACS represents the effective area of an atom that interacts with photons via the photoelectric effect, Compton scattering and pair production [16]. It is calculated by summing up the cross sections for all possible interaction mechanisms occurring within the material, and can be obtained as Eq. (14) [16]:

$$\sigma_a = \frac{\mu}{\rho} \times \frac{A}{N_A} \tag{14}$$

Where N_A is the Avogadro's number (6.022×10²³ atoms/mol), A is the atomic weight of the shielding material (g/mol), σ_a is the atomic cross section and ρ is the density of the material.

Eq. (14) indicates that the total atomic cross section is directly proportional to the MAC and is influenced by the atomic weight of the shielding material.

However, atomic cross section can also be expressed as Eq. (15) [19]:

$$\sigma_a = \frac{1}{N_A} \sum_i f_i A_i \left(\frac{\mu}{\rho}\right)_i \tag{15}$$

Where A_i is the atomic weight of every element in the target, $\left(\frac{\mu}{\rho}\right)_i$ is the MAC of the i-th element in cm²/g and f_i is the fractional abundance of the i-th element.

2. 7. Electronic Cross-Section (ECS)

It represents the probability of interaction between photons and the electrons within a material. It is the effective interaction area per electron, and primarily depends on the electron density of the material and the energy of the radiation [16]. It is expressed as Eq. (16) [16]:

$$\sigma_{el} = \frac{\mu}{\rho} \times \frac{A}{Z N_A} \tag{16}$$

where Z is the atomic number and σ_{el} is the electron cross-section.

Electronic cross-section can also be expressed as Eq. (17) [16]:

$$\sigma_{el} = \frac{1}{N_A} \sum_i \left(\frac{\mu}{\rho}\right)_i \frac{f_i w A_i}{Z_i} \tag{17}$$

where $f_i = \frac{n_i}{\sum_i n_i}$ is the fractional abundance of the i-th element, and Z_i is the atomic number of the target element.

2. 8. Effective Atomic Number (Z_{eff})

This is calculated from the atomic numbers and proportions of constituent elements in a compound or mixture. It reflects how electrons in a material respond to incoming radiation. Materials with high Z-elements tend to have high Z_{eff} . It is expressed as Eq. (18) [21]:

$$Z_{eff} = \frac{\sigma_{t,a}}{\sigma_{t,el}}$$
 (18)

where $\sigma_{t,a}$ is the total atomic cross-section and $\sigma_{t,el}$ is the total electron cross-section.

3. Results and Discussion

The radiation shielding parameters of the two classes of the selected perovskite ceramics are mainly governed by their density and were investigated to determine their usability in radiation applications. Their radiation shielding parameters are listed in Tables 1 and 2. The results obtained were discussed and are adequately based on the effects of the three most dominant interaction mechanisms: photoelectric absorption, Compton scattering and pair production.

Table 1: The density, MAC, LAC, and MFP of halide-based double perovskite

Samples	Density	MAC (cm ² /g)			LAC (cm ⁻¹)			MFP (cm)		
	(ρ)	0.015	0.2	3	0.015	0.2	3	0.015	0.2	3
	g/cm ³	MeV	MeV	MeV	MeV	MeV	MeV	MeV	MeV	MeV
Cs_2SnI_6	4.66	55.61	0.369	0.037	259.17	1.717	0.173	0.004	0.582	5.776
Cs_2TiI_6	4.49	55.72	0.363	0.037	250.21	1.628	0.167	0.004	0.614	6.004
Cs_2ZrI_6	4.54	54.04	0.361	0.037	245.34	1.640	0.169	0.004	0.610	5,933
Cs ₂ HfI ₆	4.88	67.35	0.427	0.038	328.69	2.083	0.184	0.003	0.480	5.443
Cs ₂ TeI ₆	4.59	56.00	0.370	0.037	257.05	1.699	0.17	0.004	0.589	5.878
Cs_2PtI_6	5.26	72.79	0.456	0.038	382.87	2.398	0.199	0.003	0.417	5.017
Cs ₂ PdI ₆	4.89	54.82	0.365	0.037	268.07	1.785	0.182	0.004	0.560	5.501

Table 2: The density, MAC, LAC, and MF of inorganic halide perovskite.

Samples	Density	MAC (cm ² /g)			LAC (cm ⁻¹)			MFP (cm)		
	(ρ) g/cm ³	0.015 MeV	0.2 MeV	3 MeV	0.015 MeV	0.2 MeV	3 MeV	0.015 MeV	0.2 MeV	3 MeV
CH ₃ NH ₃ PbI ₃	4.092	71.18	0.566	0.039	291.31	2.317	0.160	0.003	0.432	6.243
CH ₃ NH ₃ PbBr ₃	3.554	104.34	0.534	0.039	370.69	1.897	0.138	0.003	0.527	7.232
CH ₃ NH ₃ SnI ₃	3.649	49.95	0.344	0.037	182.27	1.255	0.136	0.005	0.797	7.239
$HC(NH_2)_2SnI_3$	3.566	48.40	0.341	0.038	172.60	2.215	0.137	0.006	0.823	7.306
$HC(NH_2)_2PbI_3$	4.101	69.27	0.558	0.040	284.14	1.286	0.164	0.004	0.437	6.103

3. 1. Halide-based Double Perovskite

In the low energy region (0.015 - 0.1 MeV) where the photoelectric effect dominates, the MAC values were highest for all samples. They reduced sharply with the rise in photon energy, as shown in Fig. 1. This was because the photoelectric cross-section varies approximately with Z^{4-5}/E^3 . However, at 0.04 MeV, it was observed that MAC values for all the studied samples showed a sharp rise due to the photoelectric effect absorption edge (K-absorption edge) of the elements present in the samples, whose Kedge energies lay just below 0.04 MeV. This led to a sharp rise in MAC values (12.163 -22.217, 8.635 - 21.635, 10.115 - 21.630, 10.608 - 20.658, 8.703 - 22.331, 11.610 - 20.929, and 11.232 - 21.939 g/cm³). As the photon energy increases above 0.04 MeV, the probability of the photoelectric absorption drops rapidly (because of the $1/E^3$ dependence), and Compton scattering begins to dominate at intermediate energies (0.2 -3 MeV). A decrease in MAC values was observed, but they remained relatively stable and less dependent on the atomic number compared to the photoelectric effect region. However, at high photon energies (>3 MeV), where pair production becomes significant, MAC values increased slightly, depending on the atomic number of the constituent elements. As a result, the reduction in attenuation values occurred as photon energies increased [13]. It is reported that halide-based double perovskites are closely governed by the atomic number of the metal center and the energy of the incident photon, which strongly influence the MAC values. So, high-Z samples (Hf, Pt, Te) contributed more to the MAC, particularly in the low energy region, which is why Cs_2PtI_6 (Z = 78), Cs_2HfI_6 (Z = 72) and Cs_2Tel_6 (Z = 52) exhibited the highest MAC values in the photoelectric

region, which amplified photoelectric interaction. Whereas Cs_2TiI_6 (Z=22) showed the lowest MAC values, as Ti has the smallest Z among the studied samples. Therefore, Cs_2PtI_6 is the best material for shielding against photon radiation.

LAC is directly proportional to both MAC and density ($\mu = \mu_m \rho$); it describes the material's actual ability to attenuate radiation per unit thickness. LAC depends on the atomic number, the energy of the incident photon, and the density of the samples. At the low energy region, a sharp decrease in the LAC values was observed with the rise in photon energy as a result of the strong inverse dependence on photon energy ($\propto E^{-3}$), as shown in Fig. 2. However, at 0.04 MeV, it was observed that the LAC values for all the studied samples gave a sharp rise due to the photoelectric effect absorption edge (Kabsorption edges) of the elements present in the samples. This led to a sharp increase in LAC values (56.680 - 103.532, 38.772 - 97.141, 45.920 - 98.201, 51.769 - 100.811, 39.949 - 102.498, 61.101 - 110.087, and 54.923 - 107.280 cm⁻¹). Compton scattering begins to dominate at intermediate energies, and a gradual decrease in LAC values was observed; these values became relatively stable and less dependent on the atomic number compared to the photoelectric effect region. At energies above 5 MeV, when pair production becomes significant, there was a slight increase in LAC in the high-Z materials [13]. It has been reported that attenuation behavior is not only energy-dependent but also material-specific, governed by the atomic number of the central metal and its density. Due to the enhanced photoelectric effect, high-Z materials (Pt, Hf, Te) showed the highest LAC values, particularly in the low energy region. At 0.1-1.5 MeV, differences in LAC values began to narrow, although higher-Z and denser materials still performed better; Cs₂PtI₆ and Cs₂HfI₆ retained their superiority. However, at 5-15 MeV, the LAC curves increased slightly for heavy elements, but Cs₂PtI₆ again performed better due to both their high Z and high density. Whereas Cs₂TiI₆ still remained the least effective. Moreover, due to the atomic number of Pt (Z = 78) in Cs_2PtI_6 , there were more interactions between photons and the Pt atoms, resulting in fewer photons being transmitted. Therefore, as the density of perovskite material increases, the material attenuates more radiation over a given thickness. However, MAC values remain unchanged due to their density-normalized property [17, 19].

The HVLs, in the low energy region, were the lowest due to the strong photoelectric effect. Minor changes in energy resulted in a rapid increase in HVL, particularly for low-Z materials, as shown in Fig. 3. However, at 0.04 MeV, it was observed that the HVL values for all the studied samples gave a sudden fall due to the photoelectric effect absorption edge (K-absorption edges) of the elements present in the samples. This led to a sudden fall in HVL values (0.012 - 0.007, 0.018 - 0.007, 0.015 -0.007, 0.013 - 0.007, 0.0017 - 0.007, 0.011 - 0.006, and 0.013 - 0.006 cm). In the intermediate energy region, HVL values increased more gradually, reflecting the dominance of Compton scattering. In the high energy region, HVL continued to rise, but less sharply for high-Z materials due to the onset of pair production, which contributed to attenuation. At 0.015 MeV, Cs₂PtI₆ has the lowest HVL (0.002 cm), indicating superior attenuation performance. Whereas, Cs₂TiI₆ exhibited the highest value of HVL (0.003 cm), requiring thicker layers to achieve the same attenuation. At 0.1 MeV, HVL values increased sharply for all samples, particularly for those with low-Z metal centers. Between 0.5 and 2 MeV, the difference in HVL values narrowed, but Cs₂PtI₆ and Cs₂HfI₆ still maintained a lower HVL than other samples, as shown in Fig. 3. Above 5 MeV, HVL values increased more slowly since HVL is inversely proportional to LAC and strongly influenced by both the atomic number of the central metal atoms and the density.

From Fig. 4, it is observed that all studied samples followed the same change pattern of TVL values with increasing energy. In the low energy region, TVL values were the lowest as a result of the strong photoelectric effect. A minor increase in photon energy

caused a sharp rise in TVL values. So, Cs_2PtI_6 displayed the lowest TVL values in this region as a result of its density $(5.26g/cm^3)$ and the high-Z of the Pt element (Z=78), which enhances the photoelectric interactions. While Cs_2TiI_6 showed the highest TVL values as a result of its density (4.49 g/cm^3) and the relatively low-Z of the Ti element (Z=22). However, at 0.04 MeV, the TVL values for all the studied samples exhibited a sudden fall due to the photoelectric absorption edge (K-absorption edge) of the elements present in the samples. This led to a sharp rise in TVL values (0.041 - 0.022, 0.059 - 0.024, 0.050 - 0.023, 0.044 - 0.023, 0.058 - 0.022, 0.038 - 0.021 and 0.042 - 0.021 cm). In the intermediate energy region, TVL values increased more gradually with moderate differentiation among the samples, which was governed by Compton scattering due to the lower attenuation coefficient, but Cs_2PtI_6 still maintained better shielding, and showed a less pronounced rise due to the onset of pair production. In the high energy region, where pair production becomes significant, TVL values were generally the highest across all samples as interaction probabilities decreased.

Therefore, the order of shielding performance (low to high TVL) is as follows: $Cs_2PtI_6 < Cs_2HfI_6 < Cs_2PdI_6 < Cs_2SnI_6 < Cs_2TeI_6 < Cs_2TeI_6 < Cs_2TeI_6$. This indicates that Cs_2PtI_6 offered superior photon shielding with the lowest TVL across all energies as a result of the highest density and the heavy Pt content; Cs_2TiI_6 displayed the poorest performance with the lightest center (Ti) and lowest density. Cs_2HfI_6 and Cs_2PdI_6 followed Pt-based compound in performance as a result of its relatively high-Z and density; Cs_2SnI_6 , Cs_2TeI_6 and Cs_2ZrI_6 displayed intermediate behaviour. Therefore, the studied perovskite samples, especially those with heavy-metal centers Cs_2PtI_6 and Cs_2HfI_6 are promising lead-free radiation shielding materials.

Low MFP values suggest that the material has superior attenuation properties. At the low energy region, where the photoelectric effect is dominant, Cs₂PtI₆ showed the lowest MFP, which indicates excellent photon absorption as a result of high density (5.26 g/cm^3) and the presence of the heavy Pt element (Z = 78). While Cs₂TiI₆ exhibited the highest MFP as a result of its density (4.49 g/cm^3) and the low-Z Ti element (Z = 22), as shown in Fig. 5. However, at 0.04 MeV, it was observed that the MFP values for all the studied samples showed a sudden decrease due to the photoelectric effect absorption edges (K-absorption edge) of the elements present in the samples. This led to a sharp rise in MFP values (0.018 - 0.010, 0.026 - 0.010, 0.022 - 0.010, 0.019 - 0.010, 0.025 - 0.010,0.016 - 0.009 and 0.018 - 0.009 cm). At the intermediate energy region, Compton scattering becomes dominant, and the photon interaction probability drops, causing higher MFP values across all samples. The gap in MFP performance between the compounds narrowed, but Cs₂PtI₆ and Cs₂HfI₆ still surpassed others with consistently lower MFP values. Hence, all samples show rising MFP trends, indicating a decrease in shielding efficiency as energy increases. However, at high energy range where pair production becomes significant, MFP values remained the highest. According to shielding efficiency, the samples were ranked as follows: $Cs_2PtI_6 < Cs_2PtI_6 < Cs_2PtI_6 < Cs_2PtI_6$ < Cs₂SnI₆ < Cs₂TeI₆ < Cs₂ZrI₆ < Cs₂TiI₆, as shown in Fig. 5. Therefore, MFP values increased with photon energy, confirming that high-energy photons interact less frequently and penetrate deeper into materials.

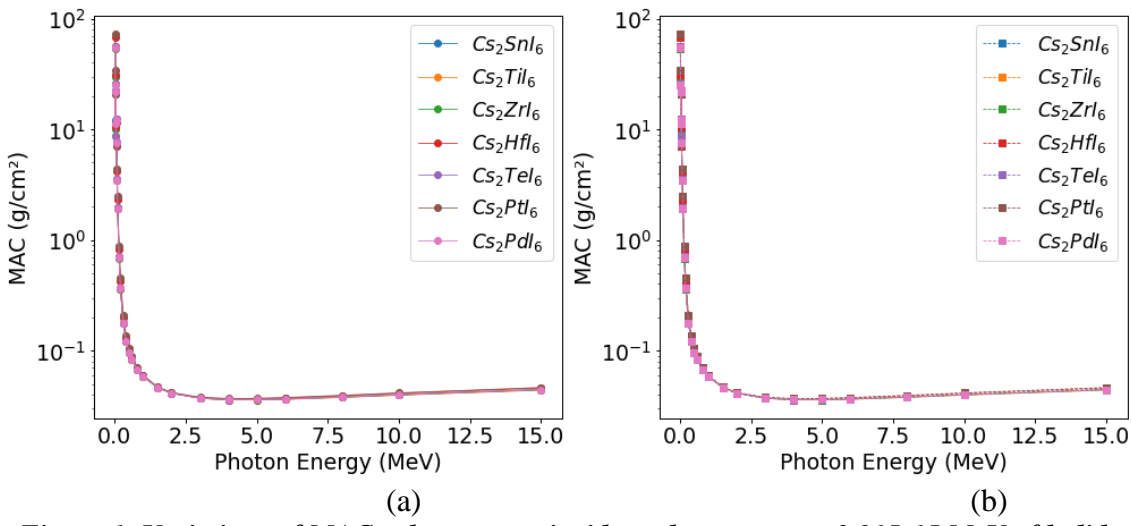


Figure 1: Variations of MAC values versus incident photon energy 0.015-15 MeV of halide based double perovskite for (a) PHY-X/PSD (b) NGCal Software.

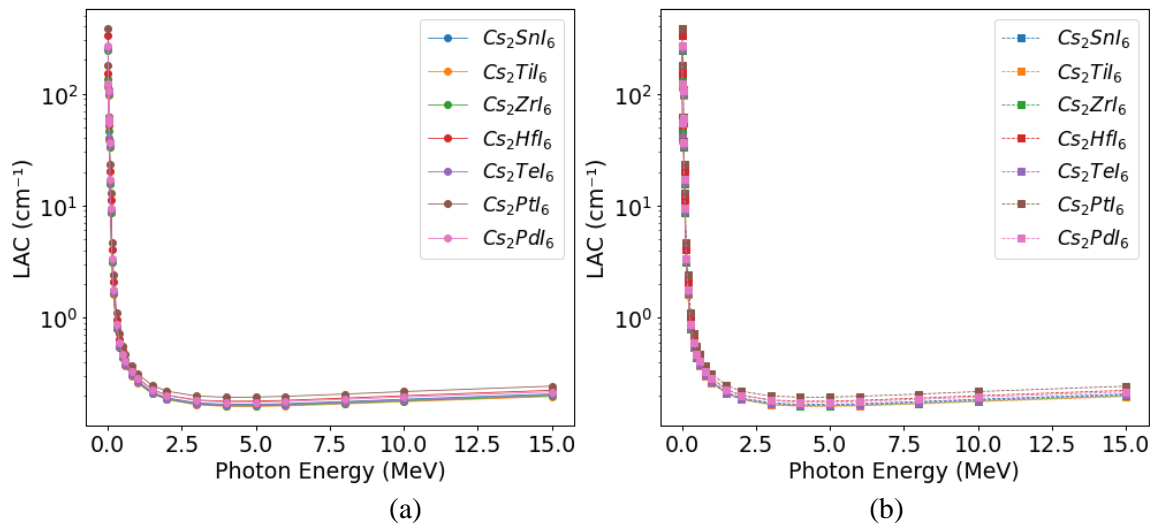


Figure 2: Variations of LAC values versus incident photon energy 0.015-15 MeV of halide based double perovskite for (a) PHY-X/PSD (b) NGCal Software.

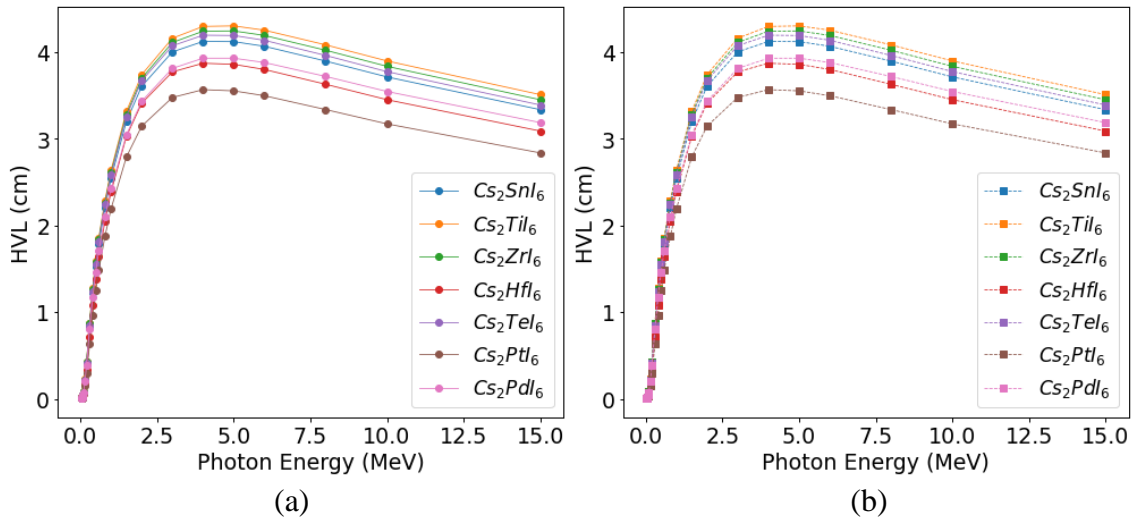


Figure 3: Variations of HVL values versus incident photon energy 0.015-15 MeV of halide based double perovskite for (a) PHY-X/PSD (b) NGCal Software.

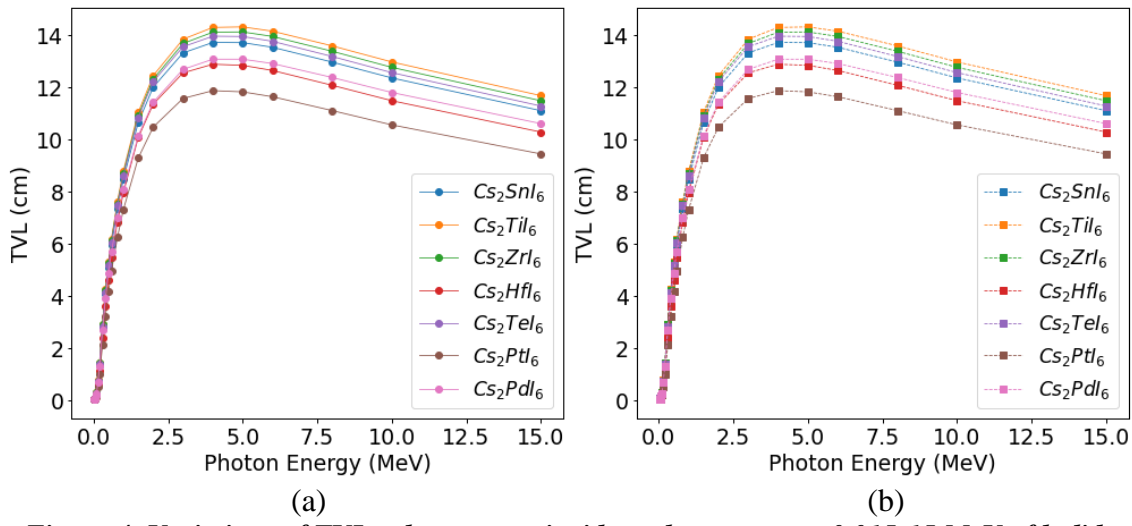


Figure 4: Variations of TVL values versus incident photon energy 0.015-15 MeV of halide based double perovskite for (a) PHY-X/PSD (b) NGCal Software.

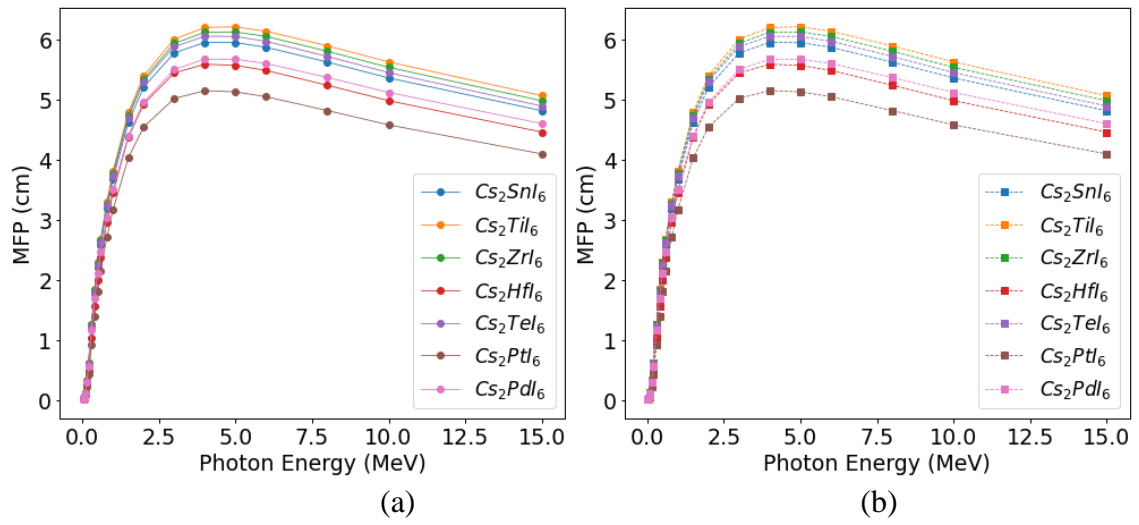


Figure 5: Variation of MFP values versus incident photon energy 0.015-15 MeV of halide based double perovskite for (a) PHY-X/PSD (b) NGCal Software.

3. 2. Organic-Inorganic Halide Perovskite

Changes of MAC values of organic-inorganic halide perovskites with photon energies in the range of 0.015-15 MeV are shown in Fig. 6. At the low energy region, where the photoelectric effect is the dominant interaction, MAC depends strongly on the atomic number (Z^4-Z^5) ; MAC values for all samples were rapidly decreasing with the increase of photon energy. However, MAC values have become large/and or small in certain energy regions as a result of differences in the absorption edges of the elements in the structure of the studied perovskite samples. Bromine (Br) has a lower Z (Z=35) than iodine (Z = 53), but the photoelectric effect depends highly on shell binding energies. Br has a K-edge at 13.47 keV, that is why it showed the highest MAC values, often greater than iodine, which has a high Z. So, between 0.015 - 0.03 MeV, Br contributed strongly due to its K-edge (13.47 keV) being near this range with MAC values of 104.303, 63.751 and 21.910 g/cm^2 . Hence, in this specific low energy, $CH_3NH_3PbBr_3$ attenuation spiked more than the iodine perovskites sample. Since lower density does not affect MAC, LAC can still be high if MAC is high enough, even with lower density. In the intermediate energy region, where Compton scattering becomes the dominant interaction, the MAC values become stable and less sensitive to atomic number. The difference in MAC values

for the different samples narrowed, but lead-based perovskites $(CH_3NH_3PbI_3)$ and $HC(NH_2)_2PbI_3$ still showed slightly higher MAC values due to increased electron density. At high energy region above 1.022 MeV, the MAC values are in the order: $CH_3NH_3PbI_3 > HC(NH_2)_2PbI_3 > CH_3NH_3PbBr_3 > CH_3NH_3SnI_3 > HC(NH_2)_2SnI_3$. The MAC values indicated that a very large number of the photons through the material were scattered, and a small number of photons were absorbed. Therefore, lead-based perovskite samples outperform tin-based. $HC(NH_2)_2PbI_3$ displayed an excellent shielding performance.

Fig. 7 shows variations in LAC values with photon energy over the range 0.015 -15 MeV. It shows a decrease in LAC with the increase in photon energy. At low energy, LAC values were highest, particularly for lead-based compounds, as a result of the heavier elements in the studied samples (high-Z content) and relative density. But it was observed that $CH_3NH_3PbBr_3$ displayed anomalously high LAC value (370.693 cm^{-1}) in the narrow energy range of around 0.015 - 0.03 MeV, where k-shell ionization of Br becomes possible. Since the K-edge of Br is around 13.47 keV (0.01347), a sharp increase in the LAC values of CH₃NH₃PbBr₃occurred just above this energy of CH₃NH₃PbBr₃. This caused a temporary peak in attenuation capability, making CH₂NH₃PbBr₃ very efficient at this narrow energy, despite its lower density and atomic number compared with iodide-based counterparts. In the intermediate energy region, LAC values decreased significantly compared to those of the low-energy region, and value differences between the samples narrowed, but lead-based materials still showed higher LAC values due to greater electron density. So, in this region, LAC values become more density-driven than Z-dependent. In the high energy region, where pair production becomes significant, the LAC values were relatively low and stable, but still slightly higher for lead-based samples. The performance difference between lead and tin-based samples remained consistent. Therefore, CH₃NH₃PbI₃ and HC(NH₂)₂PbI₃ offered superior shielding across the entire energy range. While tin-based samples (CH₃NH₃SnI₃ and HC(NH₂)₂SnI₃) displayed low attenuation performance as a result of lower-Z (Sn = 50).

Fig. 8 shows the variation in HVL values with photon energy in the range of 0.015 - 15 MeV, in which lead-based samples displayed the lowest HVL values, indicating better shielding and requiring thinner layers for effective shielding. In the low energy region (0.015 - 0.03 MeV), CH₃NH₃PbBr₃ displayed a slightly reduced HVL due to the Br K-edge (13.47 keV), leading to a temporary pick in attenuation. However, HVL values for all samples rose as Compton scattering dominated, and the differences between samples narrowed; lead-based perovskite samples still maintain better performance due to their higher electron density. While HC(NH₂)₂SnI₃ consistently displaying higher HVL values, indicating that a thicker layer is needed for effective shielding. Moreover, as pair production becomes relevant, the HVL values continued to rise as a result of the interaction probability, which contributed slightly to the attenuation of lead-based samples, making them suitable for radiation shielding across this energy range.

Fig. 9 shows the variation of TVL values with photon energy in the range 0.015 - 15 MeV, in which CH₃NH₃PbI₃ and HC(NH₂)₂PbI₃ displayed minimum values as a result of the high Z of lead in the low energy region. However, it was observed that CH₃NH₃PbBr₃ displayed a brief drop in TVL near 0.015 - 0.03 MeV as a result of Br K-edge (13.47 keV), which led to a temporary improved shielding. Tin-based samples (CH₃NH₃SnI₃ and HC(NH₂)₂SnI₃) showed high TVL values, which means less effective shielding. As the photon energy increased, Compton scattering becomes relevant and the differences between the samples TVL values decreased, but CH₃NH₃PbI₃ and HC(NH₂)₂PbI₃ still retained an edge as a result of high Z and density. Furthermore, as pair production became significant, there was a slight rise in TVL values, but

CH₃NH₃PbI₃ and HC(NH₂)₂PbI₃ still maintained the lowest TVL values, making them suitable for high photon radiation shielding.

MFP is influenced by photon energy, atomic number, density and edge effect. In the low energy region, lead-based samples showed low MFP values as a result of high Z and density, as shown in Fig. 10. However, it was observed that CH₃NH₃PbBr₃ displayed a noticeable decrease in MFP near 0.015 - 0.03 MeV, attributed to the K-edge of Br at 13.47 keV, which caused a sudden increase in attenuation, resulting in a temporary improved shielding. Hence, CH₃NH₃PbBr₃ becomes exceptionally effective at this narrow low energy level despite its low density. In the intermediate energy region, the difference in MFPs between the samples was less dependent on atomic number and more influenced by the sample's density. So, CH₃NH₃PbI₃ and HC(NH₂)₂PbI₃ still displayed lower MFP values than CH₃NH₃SnI₃ and HC(NH₂)₂SnI₃, but CH₃NH₃PbBr₃ loss it K-edge advantage beyond 0.03 MeV. As pair production becomes significant, all samples ahowed a rise in MFP values as a result of the total interaction probability. The MFP values become more stable. Shielding depends largely on electron density and overall Z-effect. Therefore, CH₃NH₃PbI₃ and HC(NH₂)₂PbI₃ still maintained the lowest MFP values, followed by CH₃NH₃SnI₃, CH₃NH₃PbBr₃ and HC(NH₂)₂SnI₃.

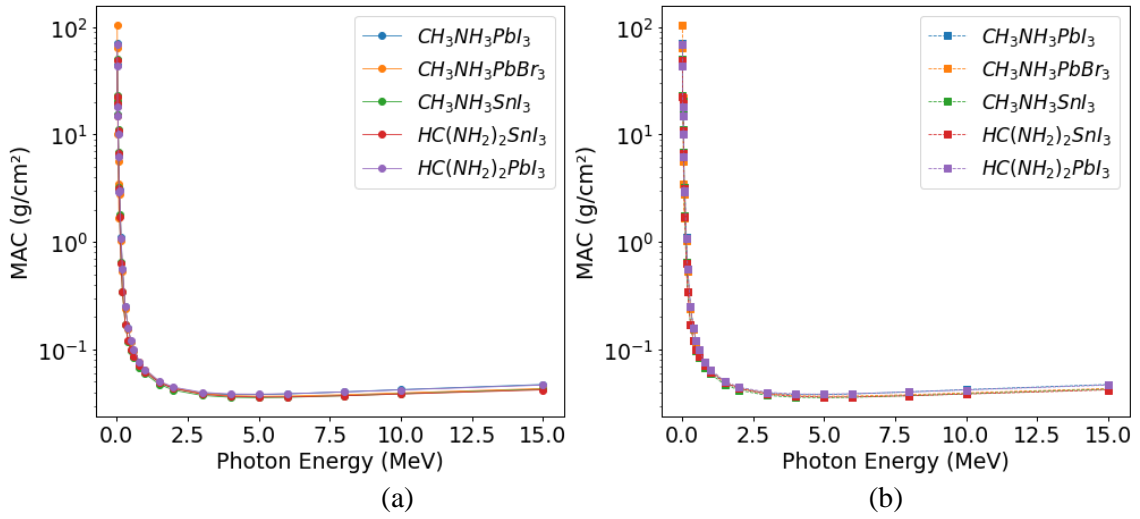


Figure 6: Variations of MAC values versus incident photon energy 0.015-15 MeV of inorganic halide perovskite for (a) PHY-X/PSD (b) NGCal Software.

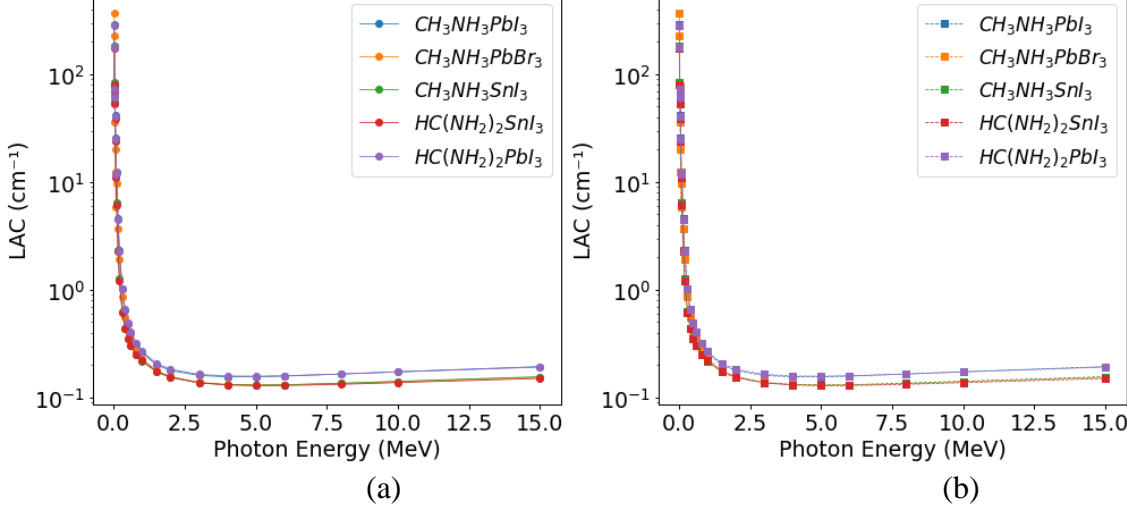


Figure 7: Variations of LAC values versus incident photon energy 0.015-15 MeV of inorganic halide perovskite for (a) PHY-X/PSD (b) NGCal Software.

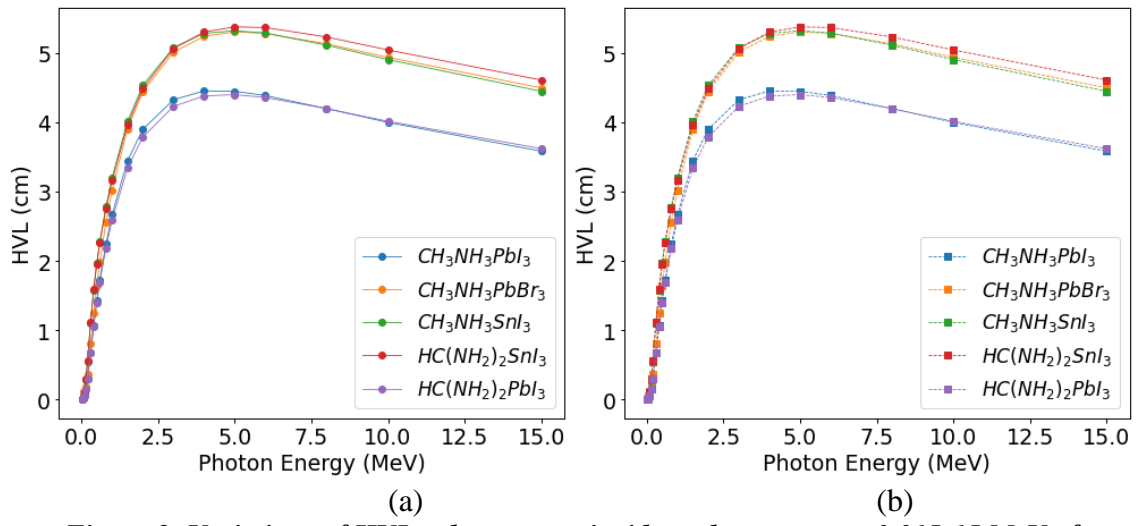


Figure 8: Variations of HVL values versus incident photon energy 0.015-15 MeV of inorganic halide perovskite for (a) PHY-X/PSD (b) NGCal Software.

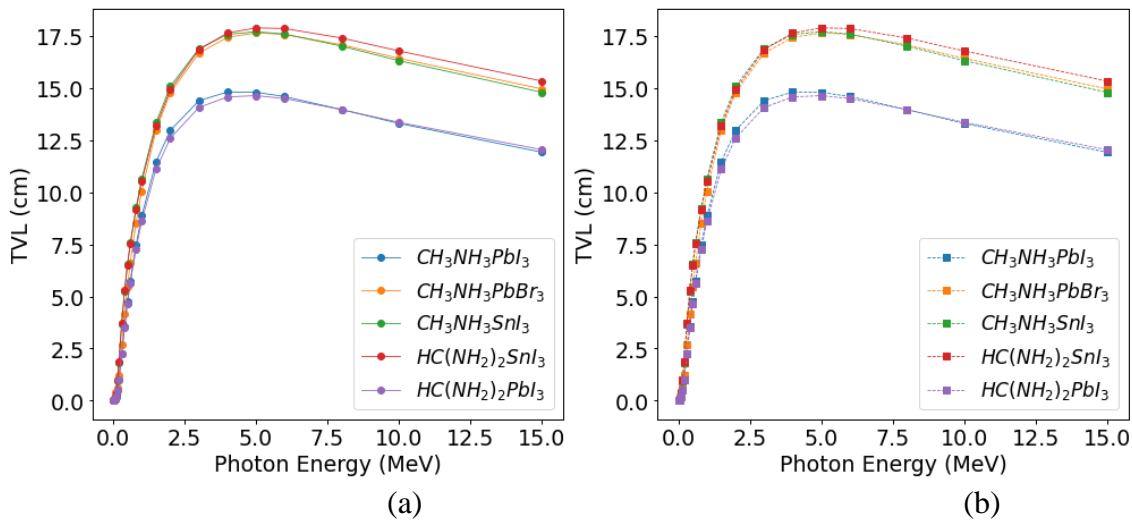


Figure 9: Variations of TVL values versus incident photon energy 0.015-15 MeV of inorganic halide perovskite for (a) PHY-X/PSD (b) NGCal Software.

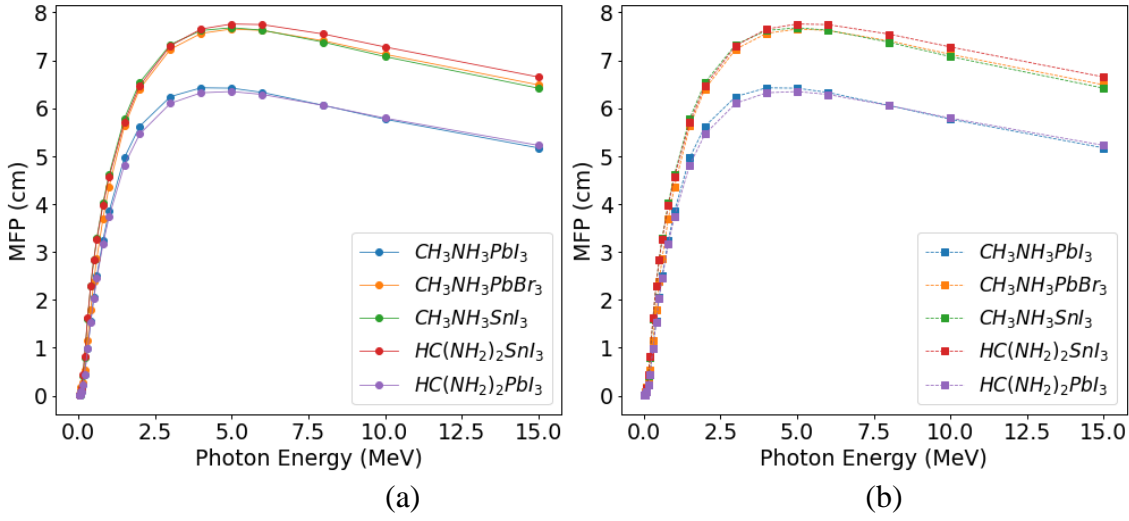


Figure 10: Variation of MFP values versus incident photon energy 0.015-15 MeV of inorganic halide perovskite for (a) PHY-X/PSD (b) NGCal Software.

Halide-based double perovskites are closely governed by the atomic number of the metal center and the energy of the incident photon [13]. They are enriched with high-Z elements (Pt, Hf, Te), demonstrating superior attenuation capabilities, particularly at the low photon energies, while organic-inorganic halide perovskites displayed moderate shielding efficiency, limited mainly by their lower density and lighter elemental composition. Yet they remained attractive due to their tunability and potential for lightweight shielding applications [12, 13, 15, 16]. Overall, halide-double perovskites offered the most promising radiation shielding performance among the studied materials, with Cs_2PtI_6 being an excellent material for photon shielding because it contains the heavy atom Pt (Z = 78), having the highest MAC and LAC values as well as the lowest HVL, TVL and MFP values across the studied energy range. Moreover, the results from the two software tools are in good agreement, differing by no more than 0.1% of the values. This trend agrees with the results reported by Şakar et al. [15], Hadil [16], and Mohammed et al. [19].

4. Conclusions

Photon radiation interaction parameters of two classes of perovskite ceramics have demonstrated promising potential as effective materials for nuclear medicine and engineering applications. The studied parameters confirmed that perovskite ceramics exhibited excellent photon attenuation abilities across the diagnostic and therapeutic energy ranges, serving as efficient shielding materials in radiotherapy rooms and imaging facilities, thereby ensuring the safety of patients, medical staff, and the surrounding environment. To make a remarkable assessment of the photon interaction possibilities of perovskite materials, the results obtained with two software were found to be in good agreement. Therefore, halide-base double perovskites demonstrated superior attenuation capabilities, particularly at low photon energies, while organic-inorganic halide perovskites displayed moderate shielding efficiency, limited mainly by lower density and lighter elemental composition, yet they remained attractive due to their tunability and potential for lightweight shielding applications.

Acknowledgement

Authors would like to thank Almighty God, the Most Gracious and the Most Merciful, for His unending grace, mercy, and blessings that saw us through the successful completion of this research work. We equally appreciate the department of Physics and Materials Science for their helping and supporting to achieve this work.

Conflict of Interest

The authors declare that they have no known competing financial interests or personal relationships that could have appeared to influence the work reported in this paper.

Funding

No fund or grant was received for conducting this study.

References

- U. C. Okonkwo, C. I. Idumah, C. E. Okafor, C. C. Ohagwu, M. E. Aronu, I. P. Okokpujie, N. N. Chukwu and C. E. Chukwunyelu, J. of Inorg. and Organo. Poly. and Mat. 32, 4093 (2022). https://doi.org/10.1007/s10904-022-02420-y.
- 2. C. V. More, Z. Alsayed, M. S. Badaw, A. A. Thabet and P.P Pawar, In Envi. Chem. Let. **19**, 2057 (2021). https://doi.org/10.1007/s10311-021-01189-9.

- 3. A. Jreije, S. K. Mutyala, B. G. Urbonavičius, A. Šablinskaitė, N. Keršienė, J. Puišo, Ž. Rutkūnienė, and Ž. D. Adlienė, Poly., **15**(7), 1 (2023). https://doi.org/10.3390/polym15071700.
- 4. F. Rouihem, M. M. Albarqi, R. A. Alsulami and F. Hosni, J. of Rad. Resea. and App. Sci. **17**(1), 100834 (2024). https://doi.org/10.1016/j.jrras.2024.100834.
- 5. W. Dridi, R.A. Alsulami, M.M. Albarqi, S. J. Alsufyani and F. Hosni, J. of Rad. Resea. and App. Sci. 17, 100805 (2024). https://doi.org/10.1016/j.jrras.2023.100805.
- H. Donya, S. Sulami, J. of the Kore. Phy. Soci. 75, 871 (2019). https://doi.org/10.3938/jkps.75.871.
- 7. E. Hannachi, K. G. Mahmoud, Y. Slimani, M. I. Sayyed, J. Arayro and Y. Maghrbi, Crys., **13**(2), 230 (2023). https://doi.org/10.3390/cryst13020230.
- 8. M. Amini, A. Vejdani-Noghreyian, A. Ebrahimi-Khankook, A. Khorsand-Zak, M. Bakaiyan, In Rom. J. of Phys. **67**, 303 (2022).
- 9. A. Sharma, S. N. Nazrin, S. A. Humaira, I. Boukhris and I. Kebaili, Rad. Phys. and Chem., **195**, 110047 (2022). https://doi.org/10.1016/j.radphyschem.2022.110047.
- 10. S. N. Nazrin, A. Sharma, S. Muhammad, N. A. Ighamdi, and S. Wageh, Rad. Phys. and Chem. **198**, 110222 (2022). https://doi.org/10.1016/j.radphyschem.2022.110222.
- 11. E. Hannachi., M. I. Sayyed, K. A. Mahmoud, Y. Slimani, S. Akhtar, B. Albarzan and A. H. Almuqrin, Applied Physics A: Mat. Sci. and Proc., 127, 970 (2021). https://doi.org/10.1007/s00339-021-05092-6.
- Y. Slimani, M. K. Hamad, I. O. Olarinoye, Y. S. Alajerami, M. I. Sayyed, M.A. Almessiere and M. H. A. Mhareb, J. of Mat. Sci.: Mat. in Electr. 32, 20867 (2021). https://doi.org/10.1007/s10854-021-06603-0.
- 13. E. A. R. Assirey, In Sau. Phar. J. 27(6), 817 (2019). https://doi.org/10.1016/j.jsps.2019.05.003.
- 14. F. Sani and S. Shafie, IOSR-JEEE 14(5), 51 (2019). https://doi.org/10.9790/1676-1405015160.
- 15. E. Şakar, B. Alim, Ö. Ö. Fırat, S.B. Ceviz, A. Baltakesmez and U. Akbaba, Rad. Phy. and Chem. **189**, 109719 (2021). https://doi.org/10.1016/j.radphyschem.2021.109719.
- 16. Hadil, MSc. thesis, Kasdi Merbah University, Algeria, 2024.
- 17. A. Sharma, M. I. Sayyed, O. Agar and H. O. Tekin, Res. in Phy. **13**, 102199 (2019). https://doi.org/10.1016/j.rinp.2019.102199.
- 18. A. Sharma, B. Singh and B.S. Sandhu, Chine. J. of Ph. **60**, 709 (2019). https://doi.org/10.1016/j.cjph.2019.06.011.
- 19. M.1. Mohammed, I. S. Yahia and H. Y. Zahran, Mat. Sci. in Semicon. Proc. **169**, 107916 (2024). https://doi.org/10.1016/j.mssp.2023.107916.
- 20. A. Olaosun, C. Aborisade, D. Shian, O. Oloyede and P. Osuolale, J. of Nig. Soci. of Physi. Sci. **7**, 2 (2025). https://doi.org/10.46481/jnsps.2025.2503.
- S. F. Olukotun, S. T. Gbenu, O. F. Oladejo, M. I. Sayyed, S. M. Tajudin, A. A. Amosun, O. G. Fadodun and M. K. Fasasi, Rad. Phy. and Chem. 177, 109079 (2020). https://doi.org/10.1016/j.radphyschem.2020.109079.
- 22. J. S. Alzahrani, A. Sharma, S. N. Nazrin, Z. A. Alrowaili and M. S. Al-Buriahi, Rad. Phy. and Chem. 193,109968 (2022). https://doi.org/10.1016/j.radphyschem.2022.109968.
- 23. H. S. Gökçe, O. Güngör and H. Yilmaz, Rad. Phy. and Chem. **185**, 109519 (2021). https://doi.org/10.1016/j.radphyschem.2021.109519.
- 24. N. Khan, G. Rooh, S. Mukamil, S.A. Khattak, M. Shoaib, I. Khan, I. Ullah, T. Ahmad, S.K. Shah, K. Safeen and M. Shoaib, Rad. Phy. and Chem. 217, 111517 (2024). https://doi.org/10.1016/j.radphyschem.2024.111517.
- 25. S. Kumar, K.S. Mann, T. Singh and S. Singh, Progre. in Nucl. Ener., **134**, 103654 (2021). https://doi.org/10.1016/j.pnucene.2021.103654.
- 26. Ševčik Ph.D. thesis, Kaunas University of Technology, Lithuania, 2024.
- 27. M. Aygun and Z. Aygun, Revis. Mexi. de Fis., **69**, 4 (2023). https://doi.org/10.31349/RevMexFis.69.040401.

التحقيق الحاسوبي في معلمات حاجز إشعاع الفوتونات للسيراميك البيروفيسكايت

محمد عبدالرحيم وصنداي أجاني وواسيع يحيى 1,2 ووجودوين إغبيالي 1 قسم الفيزياء وعلوم المواد، جامعة كوارا الحكومية، ماليتي، ولاية كوارا، نيجيريا 2 قسم الفيزياء، جامعة إيلورين، إيلورين، نيجيريا

الخلاصة

يبحث هذا العمل في كفاءة حجب إشعاع الفوتون لسير اميك البير وفسكايت المختار، وذلك من خلال نمذجة حاسوبية عبر نطاق طاقة الفوتون (0.015 ميجا إلكترون فولت. تشمل المعاملات التي يهدف البحث إليها: معامل التوهين الكتلي(MAC)، ومعامل التوهين الخطي (LAC)، وطبقة نصف القيمة (HVL)، وطبقة القيمة العاشرة (TVL)، ومتوسط المسار الحر (MFP). تستند النتيجة إلى مساهمة المقطع العرضي الكلي للتفاعل بين الفوتون والمادة (db)، وقد أظهرت أن كفاءة حجب هذه المواد تتأثر بشدة بتركيبها العنصري وكثافتها وطاقة الفوتون. استُخدمت أداتان بر مجيتان، Phy-X/PSD (PSD) في الدراسة للتحقق من دقة الحسابات. وقد وُجد أن نتائج الأداتين البر مجيتين الفوتون والمادة (db) من القيم. أظهرت البير وفسكايتات المزدوجة القائمة على الهاليدات خصائص توهين فائقة عند طاقات الفوتون المنخفضة والمتوسطة، وذلك بفضل عناصر Z عالية وكثافة عالية نسبيًا. في حين أظهرت البير وفسكايتات الهاليدية العضوية-غير العضوية كفاءة حماية متوسطة، محدودة بشكل رئيسي بانخفاض كثافتها وتركيبها العنصري الخفيف، إلا أنها ظلت جذابة نظرًا لقابليتها للضبط وإمكانية استخدامها في تطبيقات الحماية خفيفة الوزن. بشكل عام، قدمت البير وفسكايت المزدوجة القائمة على الهاليدات أفضل أداء حماية الفوتون. المواد المدروسة. وبشكل خاص، تتميز تلك التي تحتوي على ذرات تقيلة مثل البلاتين (78 = Z) بكونها مرشحة ممتازة لحماية الفوتون من الجيل التالي. ينبغي أن تركز ممتازة المستقبلية على التركيب التجريبي والاستقرار طويل الأمد تحت التعرض للإشعاع، وذلك لتسريع الاستخدام العملي لسير اميكات البير وفسكايت في تطبيقات الإشعاع.

الكلمات المفتاحية بسير اميك، تدريع إشعاعي، معاملات التدريع، معامل التوهين الكتلي، معامل التوهين الخطي.